Appendix B. Supplementary information

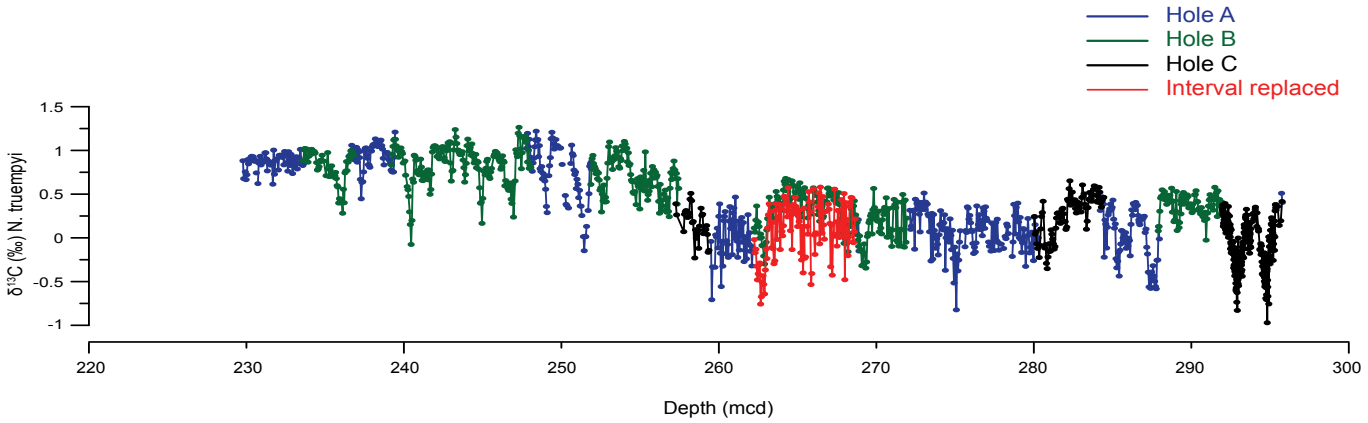

Figure S1. ODP Site 1263 benthic $\delta^{13}C$ isotope data from Hole A (blue), Hole B (green) and Hole C (black) used to construct our record. Samples in red are from Hole 1263A-26H-s2,130 to 1263A-26H-s7,20 and part of the shipboard splice (mcd; Shipboard Scientific Party, Zachos, J.C., Kroon, D. and Blum, P., et al. 2004). These samples were replaced by samples from Hole 1263B-22Hs1,0 to 1263B-22H-s5,40 (see Table S1). Part of these samples were incorporated in the revised meter composite depth (rmcd, Westerhold et al., 2007), where 208-1263A-26H-3,120 was tied to 208-1263B-22H-1,142.

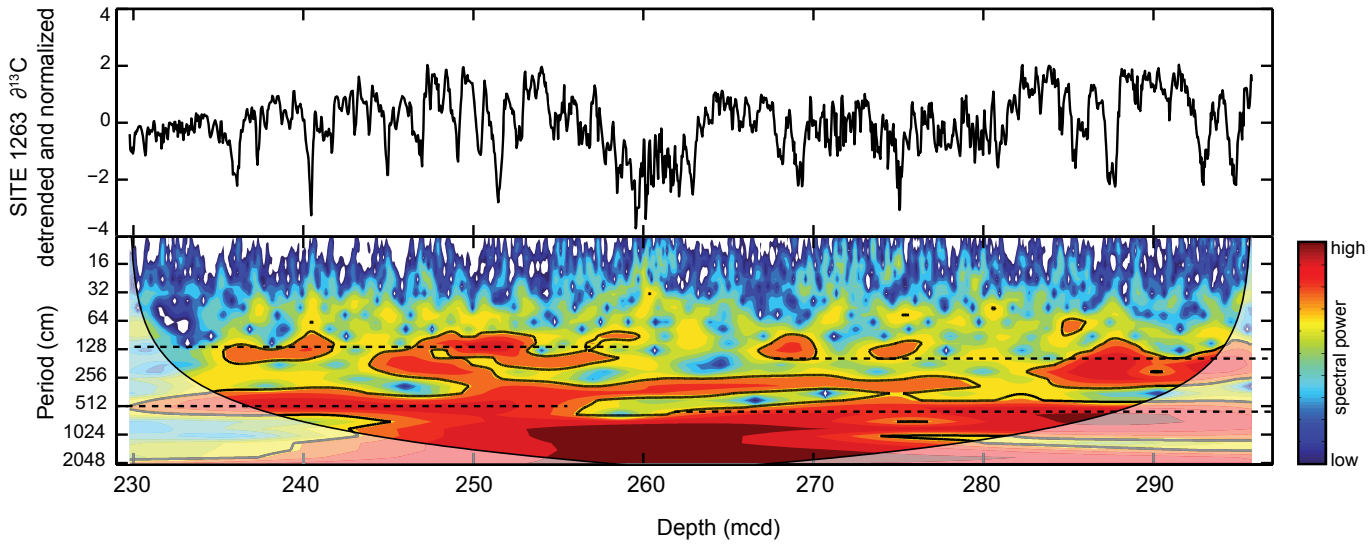

Figure S2. Evolutionary wavelet analysis of the benthic $\delta^{13}C$ record performed in the depth domain, applying a Morlet mother wavelet of order 6, and based on the wavelet script of Torrence and Compo (http://paos.colorado.edu/research/wavelets). The shaded area represents the 95% significance level. Prior to the analysis, the record was detrended and normalized. Dotted lines indicate the stronger periods in the lower and upper intervals of the record.

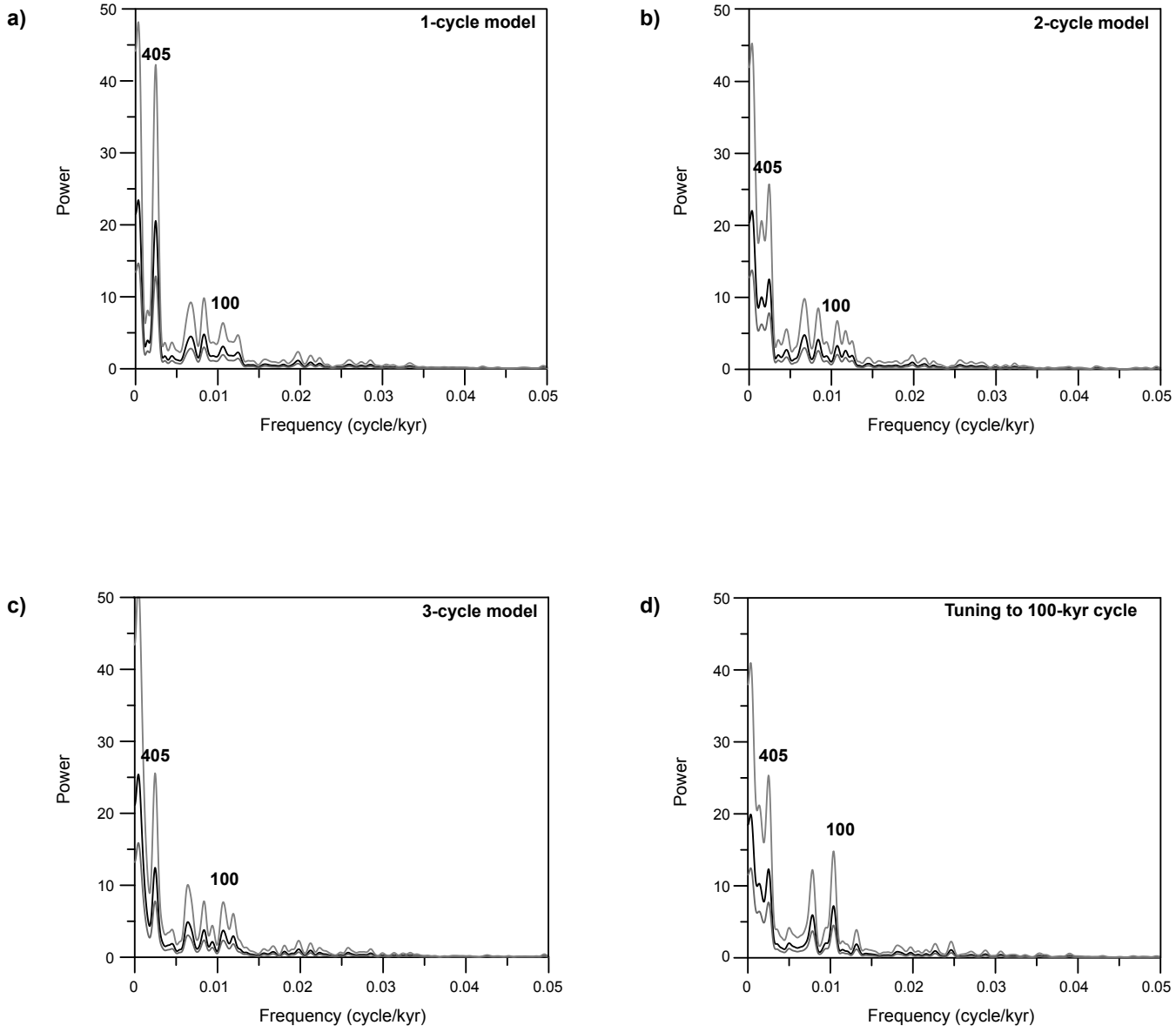

Figure S3. Power spectral analyses of the benthic $\delta^{13}C$ record based on the different age models presented. Blackman-Tuckey power spectral analysis was performed using the AnalySeries Program version 2.0.8 (Paillard et al., 1996), a Bartlett window and the confidence interval set at 80%.

Figure S4. (next page) Evolutionary wavelet analysis applied to the $\delta^{13}C$ record in the time domain, using the three age model options for the tuning to the 405-kyr cycle and the final age model based on the tuning to 100-kyr eccentricity. Wavelet spectra were obtained using the wavelet script of Torrence and Compo (http://paos.colorado.edu/research/wavelets), applying a Morlet mother wavelet of order 6. The shaded area represents the 95% significance level. Spectral power above the confidence level is concentrated at distinct frequencies, corresponding to the long 405-kyr and short eccentricity 100-kyr cycles. Prior to the analysis, the record was resampled at 3-kyr spacing, detrended and normalized.

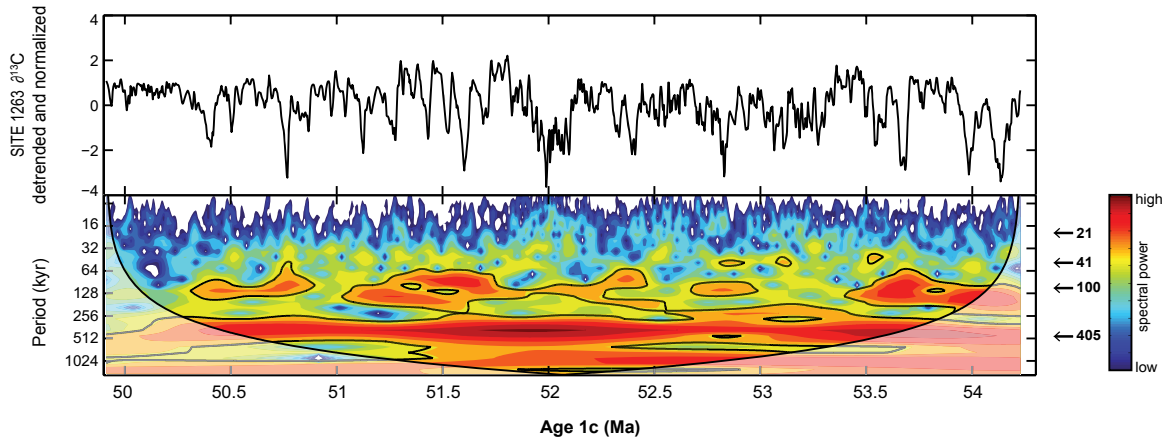
SITE 1263 δ13C detrended and normalized
4
2
0
−2
−4
Period (kyr)
16
32
64
128
256
512
1024
50
50.5
51
51.5
52
52.5
53
53.5
54
Age 1c (Ma)
high
spectral power
low
21
41
100
405

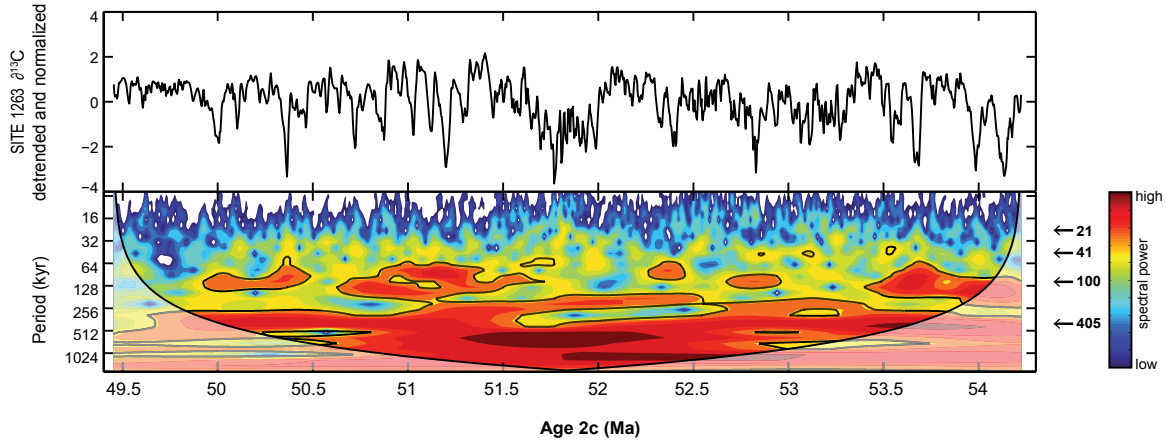
SITE 1263 δ13C detrended and normalized
4
2
0
−2
−4
Period (kyr)
16
32
64
128
256
512
1024
49.5
50
50.5
51
51.5
52
52.5
53
53.5
54
Age 2c (Ma)
high
spectral power
low
21
41
100
405

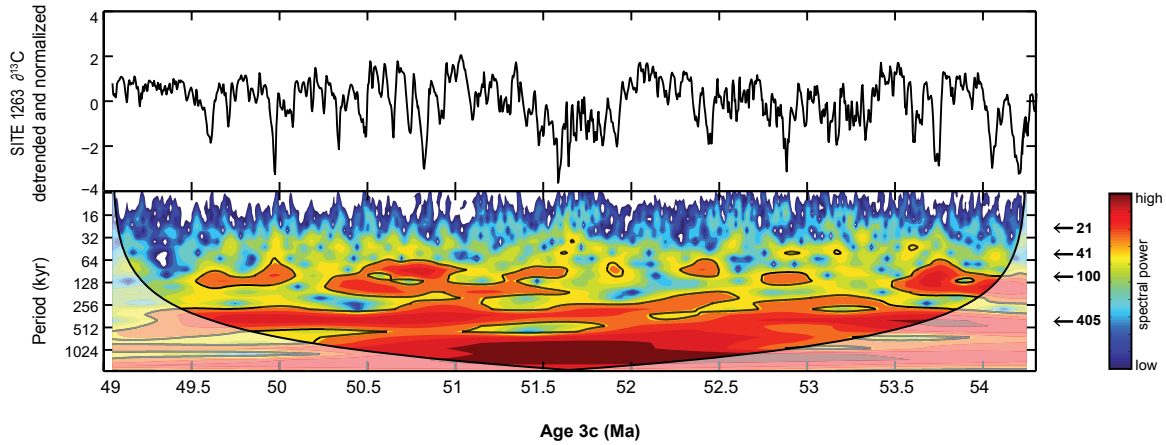
SITE 1263 δ13C detrended and normalized
4
2
0
−2
−4
Period (kyr)
16
32
64
128
256
512
1024
49
49.5
50
50.5
51
51.5
52
52.5
53
53.5
54
Age 3c (Ma)
high
spectral power
low
21
41
100
405

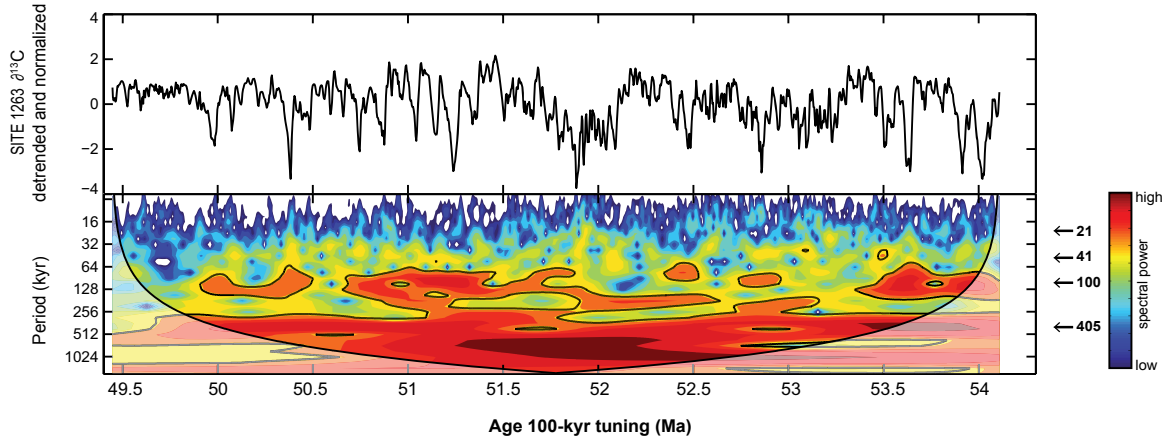
SITE 1263 δ13C detrended and normalized
4
2
0
−2
−4
Period (kyr)
16
32
64
128
256
512
1024
49.5
50
50.5
51
51.5
52
52.5
53
53.5
54
Age 100-kyr tuning (Ma)
high
spectral power
low
21
41
100
405

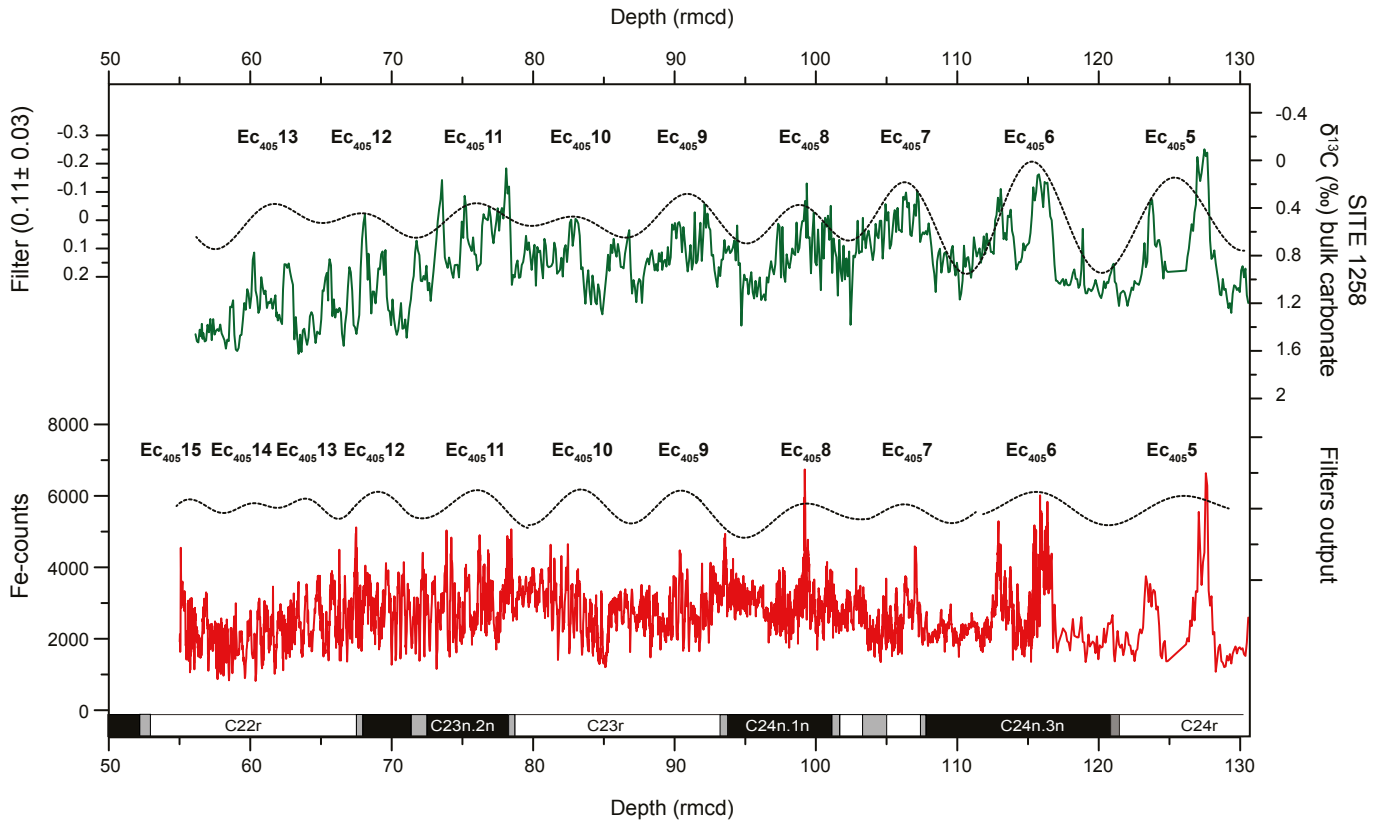

Figure S5. ODP Site 1258 bulk carbonate $\delta^{13}C$ record (Kirtland Turner et al., 2014) and high-resolution XRF Fe/intensity from ODP Site 1258 (Westerhold and Röhl, 2009). Bandpass filtering was applied in the depth domain to the XRF Fe-counts record following Westerhold and Röhl (2009) (see their Figs. 4 and 5). The comparison between the two proxies reveals coherent patterns from $Ec_{405}5$ to $Ec_{405}9$ (i.e., minima in $\delta^{13}C$ coinciding with maxima in the Fe-counts record). In the interval between $Ec_{405}10$ to $Ec_{405}15$, the problematic interpretation of $\delta^{13}C$ and Fe-counts records results in the identification of a different number of eccentricity-related cycles as well as an inconsistent phase relationship between the two proxies.